PNAS RESEARCH ARTICLE | PHYSICS OPEN ACCESS

# Activation of indistinguishability-based quantum coherence for enhanced metrological applications with particle statistics imprint

Kai Sun[a,b,1], Zheng-Hao Liu[a,b,1], Yan Wang[a,b], Ze-Yan Hao[a,b], Xiao-Ye Xu[a,b], Jin-Shi Xu[a,b,2], Chuan-Feng Li[a,b,2], Guang-Can Guo[a,b], Alessia Castellini[c], Ludovico Lami[d], Andreas Winter[e,f], Gerardo Adesso[g,h], Giuseppe Compagno[c], and Rosario Lo Franco[i,2]

Edited by Nancy Makri, University of Illinois at Urbana–Champaign, Urbana, IL; received October 28, 2021; accepted March 28, 2022, by Editorial Board Member Peter J. Rossky

**Quantum coherence, an essential feature of quantum mechanics allowing quantum superposition of states, is a resource for quantum information processing. Coherence emerges in a fundamentally different way for nonidentical and identical particles. For the latter, a unique contribution exists linked to indistinguishability that cannot occur for nonidentical particles. Here we experimentally demonstrate this additional contribution to quantum coherence with an optical setup, showing that its amount directly depends on the degree of indistinguishability and exploiting it in a quantum phase discrimination protocol. Furthermore, the designed setup allows for simulating fermionic particles with photons, thus assessing the role of exchange statistics in coherence generation and utilization. Our experiment proves that independent indistinguishable particles can offer a controllable resource of coherence and entanglement for quantum-enhanced metrology.**

identical particles | quantum coherence | quantum metrology

## Significance

Quantum coherence has a fundamentally different origin for nonidentical and identical particles since for the latter a unique contribution exists due to indistinguishability. Here we experimentally show how to exploit, in a controllable fashion, the contribution to quantum coherence stemming from spatial indistinguishability. Our experiment also directly proves, on the same footing, the different role of particle statistics (bosons or fermions) in supplying coherence-enabled advantage for quantum metrology. Ultimately, our results provide insights toward viable quantum-enhanced technologies based on tunable indistinguishability of identical building blocks.

A quantum system can reside in coherent superpositions of states, which have a role in the interpretation of quantum mechanics (1–4), lead to nonclassicality (5, 6), and imply the intrinsically probabilistic nature of predictions in the quantum realm (7, 8). Besides this fundamental role, quantum coherence is also at the basis of quantum algorithms (9–14) and, from a modern information-theoretic perspective, constitutes a paradigmatic basis-dependent quantum resource (15–17), providing a quantifiable advantage in certain quantum information protocols.

For a single quantum particle, coherence manifests itself when the particle is found in a superposition of a reference basis, for instance, the computational basis of the Hilbert space. Formally, any quantum state whose density matrix contains nonzero diagonal elements when expressed in the reference basis is said to display quantum coherence (16). This is the definition of quantum coherence employed in our work. For multiparticle compound systems, the physics underlying the emergence of quantum coherence is richer and strictly connected to the nature of the particles, with fundamental differences for nonidentical and identical particles. A particularly intriguing observation is that the states of identical particle systems can manifest coherence even when no particle resides in superposition states, provided that the wave functions of the particles overlap (18–20). In general, a special contribution to quantum coherence arises thanks to the spatial indistinguishability of identical particles, which cannot exist for nonidentical (or distinguishable) particles (18). Recently, it has been found that the spatial indistinguishability of identical particles can be exploited for entanglement generation (21), applicable even for spacelike-separated quanta (22) and against preparation and dynamical noises (23–26). The presence of entanglement is a signature that the bipartite system as a whole carries coherence even when the individual particles do not, the amount of this coherence being dependent on the degree of indistinguishability. We name this specific contribution to quantumness of compound systems "indistinguishability-based coherence," in contrast to the more familiar "single-particle superposition-based coherence." Indistinguishability-based coherence qualifies in principle as an exploitable resource for quantum metrology (18). However, it requires sophisticated control techniques to be harnessed, especially in view of its nonlocal nature. Moreover, a crucial property of identical particles is the exchange statistics, while its experimental study requiring operating both bosons and fermions in the same setup is generally challenging.

In the present work, we investigate the operational contribution of quantum coherence stemming from the spatial indistinguishability of identical particles. The main aim of our experiment is to prove that elementary states of two independent spatially indistinguishable particles can give rise to exploitable quantum coherence, with a measurable

Author contributions: K.S. and R.L.F. designed research; K.S., Z.-H.L., Y.W., Z.-Y.H., X.-Y.X., A.C., G.C., and R.L.F. performed research; K.S., Z.-H.L., Y.W., Z.-Y.H., X.-Y.X., J.-S.X., C.-F.L., A.C., L.L., A.W., G.A., G.C., and R.L.F. analyzed data; J.-S.X., C.-F.L., and G.-C.G. supervised the experimental parts of the project; R.L.F. supervised the theoretical parts of the project; and K.S., Z.-H.L., Y.W., Z.-Y.H., X.-Y.X., J.-S.X., C.-F.L., G.-C.G., A.C., L.L., A.W., G.A., G.C., and R.L.F. wrote the paper.

The authors declare no competing interest.

This article is a PNAS Direct Submission. N.M. is a guest editor invited by the Editorial Board.



[1]K.S. and Z.-H.L. contributed equally to this work.

[2]To whom correspondence may be addressed. Email: jsxu@ustc.edu.cn, cfli@ustc.edu.cn, or rosario.lofranco@unipa.it.

Published May 20, 2022.

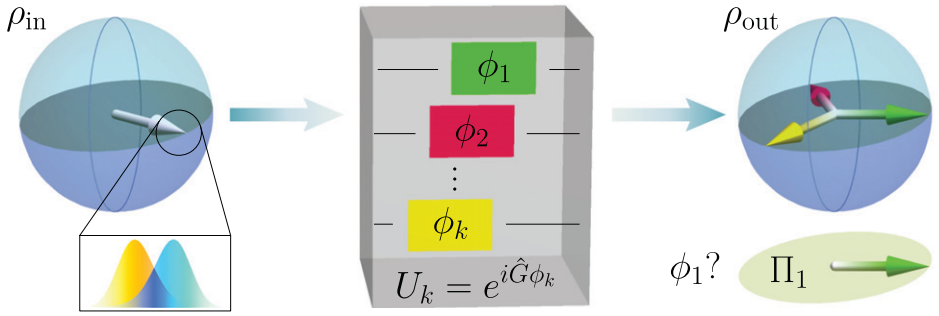


**Fig. 1.** Illustration of the indistinguishability-activated phase discrimination task. A resource state $\rho_{\text{in}}$ that contains coherence in a computational basis is generated from spatial indistinguishability. The state then enters a black box which implements a phase unitary $\hat{U}_k = e^{i\hat{G}\phi_k}, k \in \{1, \ldots, n\}$ on $\rho_{\text{in}}$. The goal is to determine the $\phi_k$ actually applied through the output state $\rho_{\text{out}}$: indistinguishability-based coherence provides an operational advantage in this task.

effect due to particle statistics. By utilizing our recently developed photonic architecture capable of tuning the indistinguishability of two uncorrelated photons (27), we observe the direct connection between the degree of indistinguishability and the amount of generated coherence and show that indistinguishability-based coherence can be concurrent with single-particle superposition-based coherence. In particular, we demonstrate its operational implications, namely, providing a quantifiable advantage in a phase discrimination task (28, 29), as depicted in Fig. 1. Furthermore, we design a setup capable of testing the impact of particle statistics in coherence production and phase discrimination for both bosons and fermions; this is accomplished by compensating for the exchange phase during state preparation, simulating fermionic states with photons, which leads to statistics-dependent efficiency of the quantum task.

## Results

**Indistinguishability-Based Coherence.** To introduce the idea of coherence activated by spatial indistinguishability (18), we start from a simple scenario where the wave functions of two identical particles with orthogonal pseudospins, $\downarrow$ and $\uparrow$, overlap at two spatially separated sites, L and R. Omitting the unphysical labeling of identical particles thanks to the no-label formalism (30), the state is described as $|\Psi\rangle = |\psi\downarrow, \psi'\uparrow\rangle$, with $|\psi\rangle = l\,|\mathrm{L}\rangle + r\,|\mathrm{R}\rangle$ and $|\psi'\rangle = l'\,|\mathrm{L}\rangle + r'\,|\mathrm{R}\rangle$ denoting the spatial wave functions corresponding to the two pseudospins. We stress that the no-label formalism adopted here proves to be well suited to our investigations requiring a tunable degree of spatial indistinguishability of identical particles. In *Materials and Methods*, we provide a more thorough discussion of the advantages of the no-label formalism in describing identical particle systems.

Let us use spatially localized operations and classical communication (the sLOCC framework) (21) to activate and exploit the operational coherence. Projecting onto the operational subspace $\mathcal{B} = \{|\mathrm{L}\sigma, \mathrm{R}\tau\rangle\,; \sigma, \tau = \downarrow, \uparrow\}$ yields the normalized conditional state (18)

$$|\Psi_{\mathrm{LR}}\rangle = \frac{1}{\mathcal{N}^{\Psi}_{\mathrm{LR}}}(lr'\,|\mathrm{L}\downarrow, \mathrm{R}\uparrow\rangle + \eta l'r\,|\mathrm{L}\uparrow, \mathrm{R}\downarrow\rangle), \qquad [1]$$

with $\mathcal{N}^{\Psi}_{\mathrm{LR}} = \sqrt{|lr'|^2 + |l'r|^2}$, and the exchange phase factor $\eta = 1\ (-1)$ originates from the bosonic (fermionic) nature of the indistinguishable particles. We see that although each particle starts from an incoherent state (namely, $|\psi\downarrow\rangle, |\psi'\uparrow\rangle$) in the pseudospin computational basis, the final state $|\Psi_{\mathrm{LR}}\rangle$ overall resembles a coherent, nonlocally encoded qubit state in the compound basis $\mathcal{B}$ under sLOCC. Also, considering that this coherence vanishes when the two particles are nonidentical and thus individually addressable (18), the emergence of coherence in $|\Psi_{\mathrm{LR}}\rangle$ essentially hinges on the spatial indistinguishability of the identical particles, in strict analogy to the emergence of entanglement between pseudospins (21, 27, 31).

The coherence of the state of Eq. **1** is independent of the bosonic or fermionic nature of the particles because of the specific choice of the initial single-particle states. However, in general, particle statistics plays a role in determining the allowed spatial overlap properties of identical particles and is thus crucial for the coherence of the overall state of the system. Hence, we shall extend our experimental investigation to a state where these fundamental aspects can be observed. Taking again a scenario with two identical particles, one of the particles is now initialized with single-particle superposition-based coherence in the pseudospin basis; i.e., the initial two-particle state reads $|\Psi'\rangle = |\psi\downarrow, \psi's'\rangle$, where $|s'\rangle = a\,|\uparrow\rangle + b\,|\downarrow\rangle$, with $|a|^2 + |b|^2 = 1$. Projecting onto $\mathcal{B}$ generates the three-level distributed state (18)

$$|\Phi_{\mathrm{LR}}\rangle = \frac{1}{\mathcal{N}^{\Phi}_{\mathrm{LR}}}(alr'\,|\mathrm{L}\downarrow, \mathrm{R}\uparrow\rangle + b(lr' + \eta l'r)\,|\mathrm{L}\downarrow, \mathrm{R}\downarrow\rangle + a\eta l'r\,|\mathrm{L}\uparrow, \mathrm{R}\downarrow\rangle), \qquad [2]$$

where $\mathcal{N}^{\Phi}_{\mathrm{LR}} = \sqrt{a^2(|lr'|^2 + |l'r|^2) + b^2|lr' + \eta l'r|^2}$. In this state, indistinguishability-based coherence coexists with single-particle superposition-based coherence, giving rise to an overall multilevel coherence in the operational basis $\mathcal{B}$.

**A Photonic Coherence Synthesizer.** We prepare two-level and three-level indistinguishability-based coherence by utilizing the photonic configuration shown in Fig. 2. The correspondence between a photon's polarization and pseudospin reads $|H\rangle \sim |\uparrow\rangle$, $|V\rangle \sim |\downarrow\rangle$, with $|H\rangle$ and $|V\rangle$ identifying horizontal and vertical polarization, respectively. As shown in Fig. 2*A*, frequency-degenerate photon pairs are generated by pumping a beamlike type II $\beta$-barium borate (BBO) crystal via spontaneous parametric down-conversion (32) and sent to the main setup via two single-mode fiber. The two-photon initial state $|H\rangle \otimes |V\rangle$ is uncorrelated, and two half-wave plates (HWPs 1 and 2) with their orientations set at 22.5° and $\theta/2$, respectively, are utilized to adjust their polarizations. Each of the two initially uncorrelated photons then passes through a polarizing beam splitter (PBS), which distributes their spatial wave functions between two remote sites, L and R, according to the polarization state. Next, additional HWPs at 45° are inserted in different paths to revert the photons' initial polarization.

The activation of functional quantum coherence from spatial indistinguishability of two photons is achieved by a beam combiner composed of a set of beam displacer (BD) arrays. A BD is a birefringent calcite crystal with a suitably cut optical axis leading

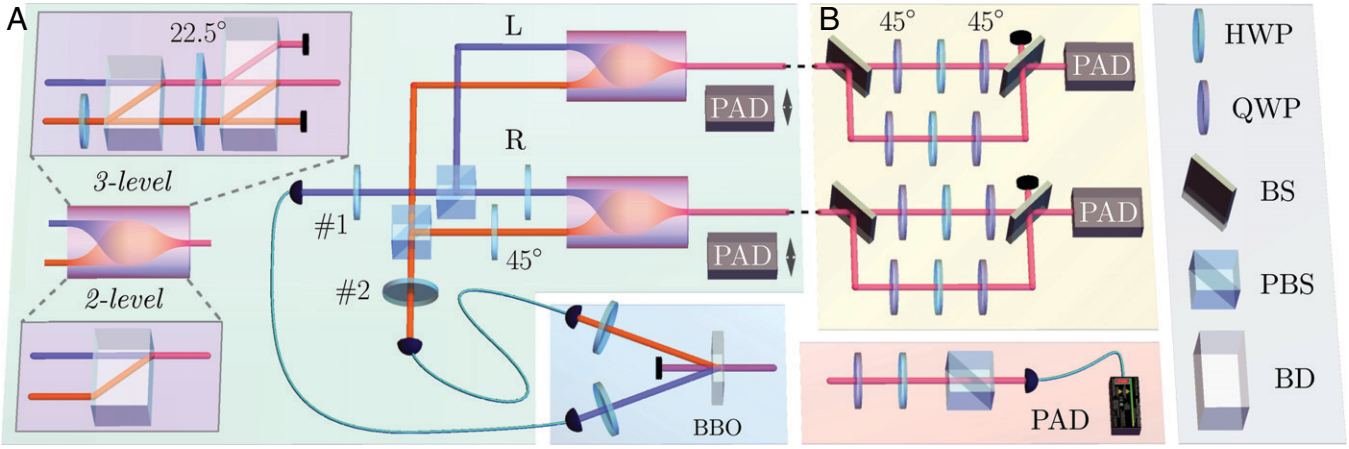


**Fig. 2.** Experimental configuration. (*A*) Preparation of coherent resource states by implementing sLOCC on indistinguishable particles. Photon pairs with orthogonal polarization states are prepared by pumping a BBO crystal. The two-photon wave functions are distributed in two spatial regions, with the indistinguishability tuned by HWPs 1 and 2. The purple boxes represent the beam combiners that are inserted to overlap the wave functions of two indistinguishable photons. (*Inset*) The detailed configuration of the beam combiner. For the activation of two-level coherence (*Lower*), a BD combines the propagating paths of the two incoming photons. For the three-level case (*Upper*), an additional HWP initializes the polarization state of one of the photons; the horizontally and vertically polarized wave function amplitudes of the photon are then successively joined in the propagating path of the other photon with a pair of BDs and an HWP in between. (*B*) Discrimination of different phases. The Franson interferometer creates two phase channels with different configurations, which are adjusted by the HWP sandwiched between two QWPs. The PAD comprises a QWP, an HWP, a PBS, and a single-photon detector.

the vertical and horizontal polarizations of photons to separate parallelly. For the preparation of the two-level state $|\Psi_{\rm LR}\rangle$, the beam combiner is composed of the setup already employed in the demonstration of polarization-entanglement activation by spatial indistinguishability (27) (Fig. 2 *A*, Lower Inset). Explicitly, a BD on each site combines the propagating directions of the two photons, in which the horizontally polarized photon is displaced while the vertically polarized photon does not change the propagating direction. At this point, the spatial wave functions of the two photons become overlapped, allowing the preparation of the state $|\Psi_{\rm LR}\rangle$ via sLOCC. A pair of polarization analysis devices (PADs) can be inserted after the beam combiner to cast polarization measurement, and the coincidence photon counting process realizes the desired projection onto the distributed basis $\mathcal{B}$. To prepare the three-level state $|\Phi_{\rm LR}\rangle$, an elaborate beam combiner setup is appended on each site, L and R (Fig. 2 *A*, Upper Inset). We defer the detailed description and setup mechanisms to *Materials and Methods*.

As a first observation, we want to prove the direct quantitative connection between produced coherence and spatial indistinguishability of photons, in analogy to what has been done for the entanglement (27). In fact, in the present experimental study, the resource of interest is quantum coherence; such a preliminary analysis is essential in view of its controllable exploitation for the specific quantum metrology protocol. This analysis is performed for the two-level state $|\Psi_{\rm LR}\rangle$ resulting from the original elementary state $|\Psi\rangle$. Various methods have been proposed to quantify coherence (28, 33–36). Here we adopt the $\ell_1$ norm of the density matrix $\rho$, that is, $C_{\ell_1}(\rho)=\sum_{i\neq j}|\rho_{ij}|$ (33). The system is prepared in $|\Psi_{\rm LR}(\theta)\rangle=\cos\theta\,|{\rm L}\uparrow,{\rm R}\downarrow\rangle+\sin\theta\,|{\rm L}\downarrow,{\rm R}\uparrow\rangle$, and its measure of coherence in the basis $\mathcal{B}$ is $C_{\ell_1}(\Psi_{\rm LR})=|\sin 2\theta|$. The coherence completely stems from the indistinguishability of the photons as it vanishes at $\theta=k\pi/2$ ($k$ is an integer), i.e., when the two photons are distinguishable.

To quantify the spatial indistinguishability of the two photons we use the entropic measure (23) $\mathcal{I}=-\sum_{i=1}^{2}p_{\rm LR}^{(i)}\log_2 p_{\rm LR}^{(i)}$, where $p_{\rm LR}^{(1)}=|lr'/\mathcal{N}_{\rm LR}^{\Phi}|^2$ ($p_{\rm LR}^{(2)}=|l'r/\mathcal{N}_{\rm LR}^{\Phi}|^2$) refers to the probability of finding the photon from $\psi$ and $\psi'$ ($\psi'$ and $\psi$) ending at L and R, respectively. For our setup, one has $\mathcal{I}=-\cos^2\theta\log_2(\cos^2\theta)-\sin^2\theta\log_2(\sin^2\theta)$. The experimental result for the measurement of coherence versus indistinguishability is plotted in Fig. 3*A*, clearly revealing the monotonic dependence in accord with theoretical predictions. Fig. 3 *A*, Inset, shows the result of quantum state tomography at $\theta=\pi/4$, which has a fidelity of 0.988 to the maximally coherent state. Hereafter, the error bars represent the $1\sigma$ SD of data points, which is deduced by assuming a Poisson distribution for counting statistics and resampling over the collected data (37). The Poisson-type uncertainty propagation method is widely adopted in the error estimation of various photonic experimental contexts, e.g., the test of nonlocal realism (38), boson sampling (39), integrated photonics (40), and fiber-based scenarios (41).

**Phase Discrimination.** Having generated tunable coherence using sLOCC, we apply it in the phase discrimination task to demonstrate the operational advantage due to indistinguishability and the role of particle statistics. The formal definition of the phase discrimination task is as follows: a phase unitary among $n$ possible choices $U_k=e^{i\hat{G}\phi_k}$, $k\in\{1,\ldots,n\}$ is randomly applied on an initial state $\rho_{\rm in}$ with a probability of $p_k$, where the generator of the transformation $\hat{G}=\sum_{\sigma\tau=\uparrow,\downarrow}\omega_{\sigma\tau}\,|{\rm L}\sigma,{\rm R}\tau\rangle\langle{\rm L}\sigma,{\rm R}\tau|$ is diagonal on the computational basis ($\omega_{\sigma\tau}$ are arbitrary coefficients) and $\sum_{k=1}^{n}p_k=1$. We shall identify the $\phi_k$ that is actually applied with maximal confidence from the output state $\rho_{\rm out}$, by using positive operator-valued measurements (POVMs). Here we focus on the simplest setting of $n=2$, with $\phi_1=0$, $\phi_2=\phi$, and solve the task using the experimentally feasible minimum-error discrimination (42, 43).

We first investigate phase discrimination with a two-level state and, without loss of generality, choose the generator $\hat{G}=|{\rm L}\uparrow,{\rm R}\downarrow\rangle\langle{\rm L}\uparrow,{\rm R}\downarrow|$ (obtained fixing $\omega_{\uparrow\downarrow}=1$ and $\omega_{\uparrow\uparrow}=\omega_{\downarrow\uparrow}=\omega_{\downarrow\downarrow}=0$). Consequently, the output states after being affected by $U_k$ read

$$|\Psi^k\rangle=\frac{1}{\mathcal{N}_{\rm LR}^{\Psi}}(lr'\,|{\rm L}\downarrow,{\rm R}\uparrow\rangle+\eta l'r e^{i(k-1)\phi}\,|{\rm L}\uparrow,{\rm R}\downarrow\rangle),\quad [3]$$

and they are discriminated by a POVM (in this case a von Neumann projective measurement) comprising two projectors

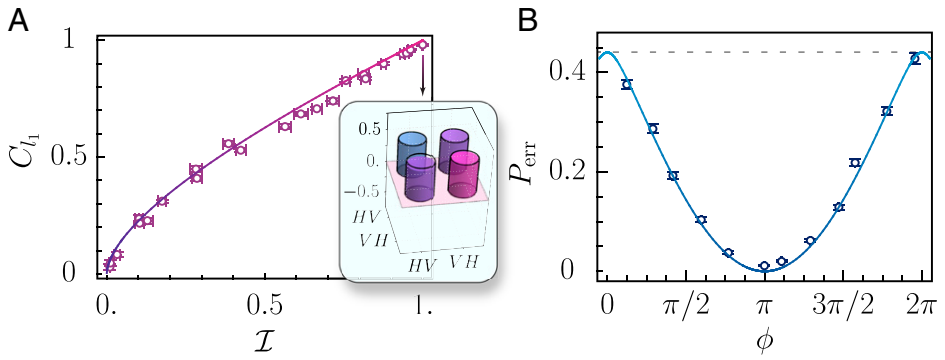


**Fig. 3.** Experimental result for the two-level state $|\Psi_{\rm LR}\rangle$. The points and curves represent experimental results and theoretical predictions, respectively. (*A*) Quantification of coherence $C_{\ell_1}$ versus the two-photon indistinguishability $\mathcal{I}$. (*Inset*) The real part of the density matrix for the input state $|\Psi_{\rm LR}(\pi/4)\rangle$ deduced by quantum state tomography. The basis correspondences read $|HV\rangle \sim |{\rm L}\uparrow, {\rm R}\downarrow\rangle$, $|VH\rangle \sim |{\rm L}\downarrow, {\rm R}\uparrow\rangle$. (*B*) The error probability $P_{\rm err}$ of phase discrimination versus the phase parameter $\phi$, with $\theta = \pi/4$ to give maximal coherence and $p_1 = 0.44$. The dashed line shows the Helstrom–Holevo bound without coherence.

$\mathbf{\Pi} = \{\hat{\Pi}_1, \hat{\Pi}_2\}$: when $\hat{\Pi}_k$ clicks, the phase is identified as $\phi_k$. By this definition, the chance of making an error is $P_{\rm err} = p_1\langle\Psi^1|\hat{\Pi}_2|\Psi^1\rangle + p_2\langle\Psi^2|\hat{\Pi}_1|\Psi^2\rangle$ and is lower bounded by the Helstrom–Holevo bound (44, 45), namely, $P_{\rm err} \geqslant \frac{1}{2}\left(1 - \sqrt{1 - 4p_1p_2\,|\langle\Psi^1|\Psi^2\rangle|^2}\right)$. For a two-level coherent state, it is straightforward to identify the measurement projectors $\hat{\Pi}_1$ and $\hat{\Pi}_2$ (18).

The phase discrimination game is experimentally realized using the setup of Fig. 2*B*. The photons in the state $|\Psi_{\rm LR}\rangle$ on the site R are sent into an unbalanced Mach–Zehnder interferometer (UMZI), while the photons on the site L are directly detected. We put an HWP between two quarter-wave plates (QWPs) fixed at 45° to build a phase gate and place one phase gate into each of the arms after a nonpolarization beam splitter (BS). In the short arm of UMZI, the choice of the phase gate angle leaves the state $|\Psi_{\rm LR}\rangle$ unchanged, while in the long arm, a relative phase $\phi$ between $|{\rm L}\downarrow, {\rm R}\uparrow\rangle$ and $|{\rm L}\uparrow, {\rm R}\downarrow\rangle$ is imported. A movable shutter (not shown) is placed in one of the arms to adjust the parameters $p_1$ and $p_2$. After the UMZI, the photons are projected on the desired state. Since $|\Psi_{\rm LR}\rangle$ is a two-level coherent state, the measurement projectors $\hat{\Pi}_1$ and $\hat{\Pi}_2$ defined in the basis $\{|{\rm L}\downarrow, {\rm R}\uparrow\rangle, |{\rm L}\uparrow, {\rm R}\downarrow\rangle\}$ are realized in the corresponding subspace from the product (single-particle) state measurement. This procedure is as follows. On the site L (R), the polarization projector is $\hat{O}_{\rm L} = |\chi\rangle\langle\chi|$ with $|\chi\rangle = \alpha|\uparrow\rangle + \beta|\downarrow\rangle$ ($\hat{O}'_{\rm R} = |\chi'\rangle\langle\chi'|$ with $|\chi'\rangle = \alpha'|\uparrow\rangle + \beta'|\downarrow\rangle$). The product projector is thus $\hat{O}_{\rm L} \otimes \hat{O}'_{\rm R}$, leading to the two-photon projector $|\Psi_{\alpha\beta}\rangle\langle\Psi_{\alpha\beta}|$ with $|\Psi_{\alpha\beta}\rangle = \alpha\beta'|{\rm L}\uparrow, {\rm R}\downarrow\rangle + \beta\alpha'|{\rm L}\downarrow, {\rm R}\uparrow\rangle$ in the subspace of interest $\{|{\rm L}\downarrow, {\rm R}\uparrow\rangle, |{\rm L}\uparrow, {\rm R}\downarrow\rangle\}$. Thanks to the final PAD unit of the setup of Fig. 2*B*, the parameters $\{\alpha, \beta, \alpha', \beta'\}$ can be adjusted to perform the desired projective measurements $\hat{\Pi}_1$ $\hat{\Pi}_2$ and eventually obtain the error probability of discrimination $P_{\rm err}$.

We directly measure the error probability of phase discrimination for various $\phi$ at $p_1 = 0.44$ by employing the maximally coherent state $|\Psi_{\rm LR}(\pi/4)\rangle$ and optimizing over the measurement settings of $\hat{\Pi}_1$ and $\hat{\Pi}_2$. The experimental result, matching well with the theoretical prediction,

$$P_{\rm err} = \frac{1}{2}\left(1 - \sqrt{1 - 2p_1(1-p_1)(1+\cos\phi)}\right), \qquad [4]$$

is shown in Fig. 3*B*. Note that without coherence, the best strategy of phase discrimination is to always guess the phase with greater probability, yielding $\bar{P}_{\rm err} = p_1$ (Fig. 3*B*, top dashed line). The reduced $P_{\rm err}$ thus unravels the almost ubiquitous advantage of indistinguishability-based coherence.

**Emulating Different Particle Statistics.** The symmetric form of Eq. **3** prevents the exchange phase factor $\eta$ from affecting the outcome of $|\Psi_{\rm LR}\rangle$-based phase discrimination task. However, when the three-level coherent state $|\Phi_{\rm LR}\rangle$ is utilized in the same task, the intrinsic statistics of the indistinguishable particles renders the situation more complicated. The bosonic nature of the photons guarantees zero exchange phase, a property both deducible from the quantum formalism and testable experimentally (46–48). Hence, the quantum states prepared in our setup naturally have $\eta = +1$. Throughout this section, we fix one of the photons at maximal superposition state $|s'\rangle = (|\uparrow\rangle + |\downarrow\rangle)/\sqrt{2}$, i.e., set $a = b$ for simplicity which is implemented with setting both HWPs, placed before the first BD in the three-level setup, to be 22.5°. Choosing the mixing parameters as $l = l' = r = r'$ ($l' = r = 0$) maximizes (destroys) the bosonic indistinguishability; this is experimentally achieved by setting the orientation of both HWPs 1 and 2 be 22.5° ($\pi/4$).

On the other hand, photonic simulations of the dynamics of fermionic (49–51) and non-Abelian anyonic systems (52) may provide additional insights for the exotic physics therein. From the observation that $\eta$ in Eq. **2** can be absorbed into $l'$, a viable investigation of fermionic systems with $\eta = -1$ can be achieved using our setup: by setting $\theta = -\pi/4$, we invert the sign of $l'$ to simulate indistinguishability-activated coherence of fermionic particles. Note that the previous simulations of fermionic or anyonic behavior via photons inevitably rely on either a highly entangled singlet state as the input state or nonlocal mathematical correspondences like Jordan–Wigner transformation to supply the antisymmetric exchange behavior. Both methods limit the scalability of simulation and scramble some topological order. In stark contrast, the applicability of our simulation method, which directly emulates the exchange properties of identical particles by harnessing the spatial indistinguishability of photons, is not limited by the above hurdles.

The prepared states emulating bosonic, distinguishable, and fermionic particles are characterized via quantum state tomography, and the results are presented in Fig. 4*A*. The three cases have fidelity of 98.4, 97.5, and 97.7%, respectively. For the bosonic case, the outcome authenticates the presence of coherence between

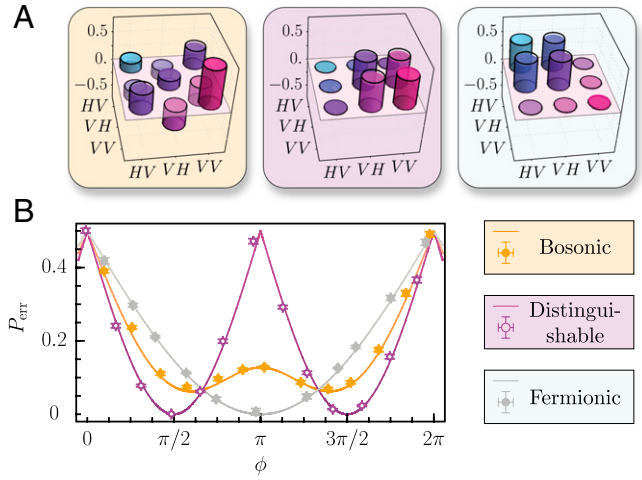


**Fig. 4.** Experimental result for three-level state $|\Phi_{\rm LR}\rangle$. (*A*) The real part of the density matrix for the input states $|\Phi_{\rm LR}\rangle$ of bosonic, distinguishable ($l'=r=0$) and fermionic particles (simulated), deduced by quantum state tomography, with $\theta=\pm\pi/4$ to give maximal coherence. The magnitudes of the imaginary part of the density matrices are smaller than 0.07. The basis correspondences read $|HV\rangle\sim|{\rm L}\uparrow,{\rm R}\downarrow\rangle$, $|VH\rangle\sim|{\rm L}\downarrow,{\rm R}\uparrow\rangle$, and $|VV\rangle\sim|{\rm L}\downarrow,{\rm R}\downarrow\rangle$. (*B*) The error probability $P_{\rm err}$ of phase discrimination versus $\phi$ for bosonic, distinguishable, and simulated fermionic particles with $p_1=0.50$. The experimental results are presented by dots with error bars in different appearances. The solid curves are the theoretical predictions with $\omega_{\downarrow\uparrow}=1$, $\omega_{\uparrow\downarrow}=2$, and $\omega_{\downarrow\downarrow}=3$.

all three vectors of the computational basis shown in Eq. **2**. For the distinguishable case ($l'=r=0$), the coherence is in contrast solely inherited from one of the particles and localized on the site R. For the fermionic case, the resulted state in Eq. **2** interestingly becomes a two-level state, $|\Psi_{\rm LR}(\pi/4)\rangle$, since the destructive interference almost completely eliminates the amplitude on the basis $|{\rm L}\downarrow,{\rm R}\downarrow\rangle$. This matches the prediction of the Pauli exclusion principle where the pseudospins of two particles are opposite. In our experiment, the exchange phase is obtained via the tomographic results as $(0.988\pm0.016)\pi$ supporting a fermion-like exchange behavior of the photons due to the compensation. Note that a minus sign appears in the coefficient of the $|{\rm L}\downarrow,{\rm R}\uparrow\rangle$ terms, which is attributed to the $\pi$-phase acquired by the photons upon reflected by PBS.

We are now in the position to investigate the role of particle statistics in the phase discrimination task. The corresponding operations $U_k$ are again realized using the phase gates within the UMZI, yielding two output states $|\Phi^k\rangle$ (18) written as

$$|\Phi^k\rangle=(a(lr'e^{i\omega_{\downarrow\uparrow}\phi_k}|{\rm L}\downarrow,{\rm R}\uparrow\rangle+\eta l're^{i\omega_{\uparrow\downarrow}\phi_k}|{\rm L}\uparrow,{\rm R}\downarrow\rangle)+b(lr'+\eta l'r)e^{i\omega_{\downarrow\downarrow}\phi_k}|{\rm L}\downarrow,{\rm R}\downarrow\rangle)/\mathcal{N}^{\Phi}_{\rm LR}. \quad [5]$$

Here we set $\omega_{\downarrow\uparrow}=1$, $\omega_{\uparrow\downarrow}=2$, and $\omega_{\downarrow\downarrow}=3$ in the generator $\hat{G}$. Unlike the two-level situation, in this three-level coherent case we need to place an UMZI on each site L and R. The UMZI has a path difference equivalent to 2.7 ns between the long and short paths, and the coincidence interval is set at 0.8 ns. The quantum states affected by the two phase operations in the UMZIs are registered separately (53, 54). We adjust the electric delay of the coincidence module to pick out the events in which the two photons had taken the long/short and short/long paths, which correspond to the state after being affected by $U_1$ and $U_2$, respectively. Moreover, for the measurement of the three-level system, to minimize the error probability of discrimination $P_{\rm err}$, three projectors $\hat{\Pi}_1$, $\hat{\Pi}_2$, and $\hat{\Pi}_3$ are required where $\Sigma_i^3\hat{\Pi}_i=I$ and ${\rm Tr}[\hat{\Pi}_3|\Phi^1_{\rm LR}\rangle\langle\Phi^1_{\rm LR}|]={\rm Tr}[\hat{\Pi}_3|\Phi^2_{\rm LR}\rangle\langle\Phi^2_{\rm LR}|]=0$. The projectors $\hat{\Pi}_i$ $(i=1,2,3)$ consist of three linearly independent basis vectors $\mathcal{B}'=\{|{\rm L}\uparrow,{\rm R}\downarrow\rangle,|{\rm L}\downarrow,{\rm R}\uparrow\rangle,|{\rm L}\downarrow,{\rm R}\downarrow\rangle\}$ (see details in *Materials and Methods*). Similarly to the method used above for the two-level state, these three projectors are also extracted from the subspace of the product projectors on the two sites L and R and implemented by the PAD unit of the setup.

Fig. 4*B* reports the measured error probabilities for phase discrimination with the three-level states. A clear discrepancy between the reliability of phase discrimination using different kinds of particles can be observed. Particularly, both types of indistinguishable particles provide advantage over distinguishable ones within the range of $\phi\in(\frac{2\pi}{3},\frac{4\pi}{3})$, but fermions further outperform bosons by a difference in $P_{\rm err}$ of 0.119 at $\phi=\pi$. This can be intuitively interpreted by recalling that the exchange interaction of fermions prevents them from occupying the same state, so the wave function amplitude disperses between different states and produces a large amount of coherence. In contrast, bosons tend to bunch on a single state, so the applicable coherence is reduced. The experimental result for the fermionic three-level case, as shown in Fig. 4*B*, appears similar but not identical to a reported two-level case given in the earlier text (Fig. 3*B*). In the experimental configuration here, the wave function amplitude of $|{\rm L}\downarrow,{\rm R}\downarrow\rangle$ vanishes due to the destructive interference when two trajectories of indistinguishable particles coalesce on the BD. Also, the two discrimination games are subject to slightly different subchannel probabilities $p_1$.

## Discussion

Coherence activated from spatial indistinguishability is a fundamental contribution to the quantumness of multiparticle composite systems intimately related to the presence of identical particles (subsystems). It cannot exist between different types of quanta, that is, in systems made of nonidentical (or distinguishable) particles. Due to its intrinsically nonlocal trait, in order to apply the indistinguishability-based coherence in quantum information tasks, transformations and measurements on the resource state must admit a product decomposition into local operations, which are achieved by sLOCC. We note that in the case of two identical particles, Schmidt decomposition recovers our capability to perform all possible measurements (55). Therefore, applying indistinguishability-based coherence between three or more quanta will be an open research route.

In this paper, we have experimentally investigated indistinguishability-based coherence, demonstrating its operational usefulness in a quantum metrology protocol. Our photonic architecture is capable of tuning the degree of spatial indistinguishability of two uncorrelated photons and adjusting the interplay between indistinguishability-based coherence and single-particle superposition-based coherence to synthesize hybrid, multilevel coherence from two nonorthogonal pseudospins. This has allowed us to prepare via sLOCC various types of resource states by devising and implementing a beam combiner and characterize the operational coherence via the phase discrimination task. Our results highlight, in a comprehensive fashion, the fundamental and practical aspects of controllable indistinguishability of identical building blocks for quantum-enhanced technologies.

In our experiment, there is no dynamical noise in the regions L and R. However, there are typical conditions where dephasing or dissipative noise become relevant, such as for long-distance or lossy environment quantum metrology tasks. In these cases, the detrimental effects to quantumness can be efficiently shielded by a sufficiently high degree of spatial indistinguishability between

particles. In fact, the selection rules intrinsically linked to particle indistinguishability are capable of both preventing the decay and enabling the recovery of quantum coherence or entanglement during the evolution (23–26).

A particularly interesting feature of our setup is that it has been devised in such a way that both bosonic and fermionic statistics can occur in the resource states, thus enabling the possibility to directly observe how the nature of the employed particles affects the efficiency of the quantum task. The present experiment also shows that within the usual first quantization approach with fictitious labels to describe identical particle states, the superpositions of a two-particle state and its permuted version enforced by the symmetrization postulate give rise to true, physical entanglement (e.g., $|\psi\downarrow,\psi'\uparrow\rangle \leftrightarrow \frac{1}{\sqrt{2}}(|\psi\downarrow\rangle_A \otimes |\psi'\uparrow\rangle_B + \eta\,|\psi'\uparrow\rangle_A \otimes |\psi\downarrow\rangle_B)$, where fictitious labels $A$ and $B$ have been adopted). This result can be seen as a confirmation of what one can deduce from a recent experiment to directly measure the statistics exchange phase of photons (46, 47), where a quantum interference between a reference state and its physically exchanged version is created. In our experiment, such an entanglement, due to the enabled quantum coherence, is entirely contained in the elementary state of two independent spatially indistinguishable photons expressed in the no-label formalism, with the particle statistics imprint emerging in the final state after the sLOCC measurement.

As the photon source in the present experiment is realized via spontaneous parametric down-conversion, its scalability appears limited due to the rapidly decreasing efficiency of the generation of the required multiphoton state. However, scalable metrological applications of indistinguishability-enabled coherence may be implemented, in prospect, by using deterministic single-photon sources (56, 57). Our experiment represents a basic proof of principle which is thus amenable to scalability.

Looking forward, it would be interesting to develop a similar experiment with actual fermions. Platforms with devices realizing linear optics operations with fermions, such as electrons, would be the best candidates. To this purpose, one may use quantum dots as sources of single electrons that can be emitted on demand (58), initialized in given spin states (59), and sent to quantum point contacts operating like electronic beam splitters (60, 61). Atomic circuits may also be employed to control single electrons (62). Our experiment thus paves the way toward suitably exploiting these different platforms to investigate indistinguishability-enabled quantum coherence with real fermions.

We finally remark that the observed phenomena in our experiment do not only follow a mapping of a fermionic state into a photonic system. Indeed, they recover fundamental traits of the original fermionic system. For example, we have observed that the $\pi$-exchange (fermionic) phase from optical compensation causes the photonic wave function on the symmetric state to vanish. This observation is in strict analogy to the Pauli exclusion principle found for real fermions forbidding multiple occupations of the same state: both these behaviors originate from the destructive interference due to the exchange of identical fermionic particles in the superposed two-particle states. Therefore, our work also constitutes an eligible quantum simulation of different kinds of identical particles and may shed further light on the characterization of this kind of compound systems, including anyons. Notably, the investigation of anyonic braiding may facilitate fault-tolerant quantum computation and information processing protocols (52, 63). To this end, our setup provides a pathway to address this problem naturally and intuitively. These studies constitute one of the main prospects motivated by the present work and will be investigated in the near future.

## Materials and Methods

In this section, we start with a comprehensive discussion of the merit of the no-label formalism in the description of identical particles. We then present the detailed procedure for generating multilevel coherence via particle indistinguishability and applying it in a quantum metrological task.

**Practical Merits of the No-Label Formalism.** The no-label formalism describing identical particles is a powerful tool suitable for various practical scenarios. Its main features are as follows: 1) it avoids fictitious labels which may complicate the analysis, 2) it directly encompasses bosons and fermions on the same footing, 3) it allows for the natural introduction of a continuous degree of spatial indistinguishability of experimentally friendly use (23), and 4) it permits is to access physical entanglement by sLOCC (21, 30).

By virtue of the no-label formalism in our analysis, the difference between the particle (statistics) exchange behaviors can be completely absorbed in a different exchange phase of the final state obtained by sLOCC. Therefore, the no-label formalism can facilitate the photonic simulation of fermionic exchange by compensation of the exchange phase. Moreover, its equivalence with the standard formalism on the mathematical level guarantees that when we map the bosonic state into the fermionic Hilbert space, the result will remain unchanged even from the viewpoint of the standard formalism (i.e., from both first quantization approach with fictitious labels and second quantization approach; see also refs. 19, 64–66). For all these reasons, the no-label formalism has been largely adopted during recent years for both theoretical and experimental analyses (27, 31, 67, 68).

**Generation of Multilevel Coherence.** Here we describe the procedure of generating the three-level, hybrid (indistinguishability- and superposition-based) coherence with beam combiner. The initial state $|\Psi'\rangle = |\psi\downarrow,\psi' s'\rangle = |\psi\downarrow,\psi'(a\uparrow + b\downarrow)\rangle$ is realized by placing another HWP before the first BD on each site, L and R, to modify the pseudospin of $|\psi'\rangle$ from $|\uparrow\rangle$ to $a\,|\uparrow\rangle + b\,|\downarrow\rangle$. This is followed further by a $\sigma_x$-compensation causing the $\psi'$ component to evolve to $b\,|\uparrow\rangle + a\,|\downarrow\rangle$ ; the effect of the compensation is also absorbed into the HWP. Inside the beam combiner, two BDs sandwiching an HWP oriented set at 22.5° at each site form a Mach–Zehnder interferometer. After the first BD in the interferometer, the photonic wave function corresponding to the first term of $b\,|\uparrow\rangle + a\,|\downarrow\rangle$, i.e., $b\,|\uparrow\rangle$, is displaced to the path of the other photon whose pseudospin is $|\downarrow\rangle$, and the remaining part $a\,|\downarrow\rangle$ passes directly. At this stage, the HWP fixed at 22.5° implements a Hadamard transformation on the spin states to erase the original path information of the two photons. The remaining part on the lower path now reads $a(|\psi'\uparrow\rangle + |\psi'\downarrow\rangle)/\sqrt{2}$, and the second BD merges its first term, $a\,|\psi'\uparrow\rangle/\sqrt{2}$, to the middle path which contains $|\psi\downarrow, b\psi'\downarrow\rangle/\sqrt{2}$. As the result, for the three output paths of the interferometer, the wave function of the upper one reads $|\psi\uparrow, b\psi'\uparrow\rangle/\sqrt{2}$, and the middle path consists of the wave function $|\psi\downarrow,\psi'(a\uparrow + b\downarrow)\rangle/\sqrt{2}$, while the remaining part, $a/\sqrt{2}\,|\psi'\downarrow\rangle$, locates in the bottom path. Thus, we only need to extract photons in the middle path, in which $|\downarrow\rangle$ and $a\,|\uparrow\rangle + b\,|\downarrow\rangle$ are combined together, and discard photons located on the other two paths (these photons do not contribute to the final counting events). Following the same measurement method introduced above, the three-level state $|\Phi_{LR}\rangle$ underpinning the system is finally activated.

**Phase Discrimination with Three-Level System.** Compared with the two-level case, some subtlety underlies the measurement of the three-level system: First, because Eq. **2** is spanned by three linearly independent basis vectors $\mathcal{B}' = \{|L\uparrow, R\downarrow\rangle, |L\downarrow, R\uparrow\rangle, |L\downarrow, R\downarrow\rangle\}$, a POVM consisting of only two rank-1 projectors cannot satisfy the requirement of completeness. As such, even the discrimination of two phases will require additional projectors. Second, the projectors that minimize the probability of committing errors are generally entangled and thus not directly viable. To resolve these issues, we construct two auxiliary projectors, orthogonal to both of the states $|\Phi^k\rangle$, to construct a POVM $= \{\hat{\Pi}_1, \hat{\Pi}_2, \hat{\Pi}_3, \hat{\Pi}_4\}$ in the direct sum dilated four-dimensional space $\mathcal{B}$, so that every element of the POVM admits the product expansion $\Pi_k = |Ls, Rs'\rangle\langle Ls, Rs'|$, with $s$ and $s'$ being the localized pseudospin states, and the POVM recovers the probability distribution on $\mathcal{B}'$. Any experimental trial that

eventuates in the detection on the auxiliary projectors is counted as an incorrect discrimination, regardless of the actual phase applied.

**Data Availability.** All study data are included in the main text.

**ACKNOWLEDGMENTS.** This work was supported by National Key Research and Development Program of China (Grant 2017YFA0304100); the Innovation Program for Quantum Science and Technology (Grant 2021ZD0301400); the National Natural Science Foundation of China (Grants 61725504, U19A2075, 61805227, 61975195, 11774335, and 11821404); Key Research Program of Frontier Sciences, Chinese Academy of Sciences (CAS) (Grant QYZDY-SSW-SLH003); Science Foundation of the CAS (Grant ZDRW-XH-2019-1); the Fundamental Research Funds for the Central Universities (Grants WK2470000026 and WK2030380017); and Anhui Initiative in Quantum Information Technologies (Grants AHY020100 and AHY060300). L.L. acknowledges support from the Alexander von Humboldt Foundation. R.L.F. is thankful for support from Sistema di Incentivazione, Sostegno e Premialità della Ricerca Dipartimentale, Dipartimento di Ingegneria, Università di Palermo.

Author affiliations: [a]Chinese Academy of Sciences Key Laboratory of Quantum Information, University of Science and Technology of China, Hefei 230026, People's Republic of China; [b]Chinese Academy of Sciences Centre for Excellence in Quantum Information and Quantum Physics, University of Science and Technology of China, Hefei 230026, People's Republic of China; [c]Dipartimento di Fisica e Chimica–Emilio Segrè, Università di Palermo, 90123 Palermo, Italy; [d]Institut für Theoretische Physik, Universität Ulm, D-89069 Ulm, Germany; [e]Institució Catalana de Recerca i Estudis Avançats (ICREA), Universitat Autònoma de Barcelona, ES-08193 Bellaterra, Spain; [f]Física Teórica: Informació i Fenómens Quàntics, Departament de Física, Universitat Autònoma de Barcelona, ES-08193 Bellaterra, Spain; [g]School of Mathematical Sciences, University of Nottingham, Nottingham NG/2RD, United Kingdom; [h]Centre for the Mathematics and Theoretical Physics of Quantum Non-Equilibrium Systems, University of Nottingham, Nottingham NG/2RD, United Kingdom; and [i]Dipartimento di Ingegneria, Università di Palermo, 90128 Palermo, Italy

1. E. Schrödinger, Die gegenwärtige situation in der quantenmechanik. *Naturwissenschaften* **23**, 823–828 (1935).
2. E. P. Wigner, "Remarks on the mind-body question" in *Philosophical Reflections and Syntheses*, J. Mehra, Ed. (Springer, 1995), pp. 247–260.
3. D. Frauchiger, R. Renner, Quantum theory cannot consistently describe the use of itself. *Nat. Commun.* **9**, 3711 (2018).
4. K.-W. Bong *et al.*, A strong no-go theorem on the Wigner's friend paradox. *Nat. Phys.* **16**, 1199–1205 (2020).
5. A. M. Gleason, Measures on the closed subspaces of a Hilbert space. *J. Math. Mech.* **6**, 885–893 (1957).
6. S. Kochen, E. P. Specker, The problem of hidden variables in quantum mechanics. *J. Math. Mech.* **17**, 59–87 (1967).
7. M. N. Bera, A. Acín, M. Kuś, M. W. Mitchell, M. Lewenstein, Randomness in quantum mechanics: Philosophy, physics and technology. *Rep. Prog. Phys.* **80**, 124001 (2017).
8. X. Yuan, H. Zhou, Z. Cao, X. Ma, Intrinsic randomness as a measure of quantum coherence. *Phys. Rev. A* **92**, 022124 (2015).
9. P. W. Shor, "Algorithms for quantum computation: Discrete logarithms and factoring" in *Proceedings 35th Annual Symposium on Foundations of Computer Science*, S. Goldwasser, Ed. (IEEE, 1994), pp. 124–134.
10. E. Martin-Lopez *et al.*, Experimental realization of Shor's quantum factoring algorithm using qubit recycling. *Nat. Photonics* **6**, 773–776 (2012).
11. R. Cleve, A. Ekert, C. Macchiavello, M. Mosca, Quantum algorithms revisited. *Proc. R. Soc. Lond. A* **454**, 339–354 (1998).
12. L. M. Procopio *et al.*, Experimental superposition of orders of quantum gates. *Nat. Commun.* **6**, 7913 (2015).
13. S. Aaronson, A. Arkhipov, "The computational complexity of linear optics" in *Proceedings of the Forty-Third Annual ACM Symposium on Theory of Computing*, L. Fortnow, S. Vadhan, Eds. (Association for Computing Machinery, New York, NY, 2011), pp. 333–342.
14. F. Arute *et al.*, Quantum supremacy using a programmable superconducting processor. *Nature* **574**, 505–510 (2019).
15. A. Winter, D. Yang, Operational resource theory of coherence. *Phys. Rev. Lett.* **116**, 120404 (2016).
16. A. Streltsov, G. Adesso, M. B. Plenio, Colloquium: Quantum coherence as a resource. *Rev. Mod. Phys.* **89**, 041003 (2017).
17. E. Chitambar, G. Gour, Quantum resource theories. *Rev. Mod. Phys.* **91**, 025001 (2019).
18. A. Castellini *et al.*, Indistinguishability-enabled coherence for quantum metrology. *Phys. Rev. A (Coll. Park)* **100**, 012308 (2019).
19. S. Chin, J. Huh, Entanglement of identical particles and coherence in the first quantization language. *Phys. Rev. A (Coll. Park)* **99**, 052345 (2019).
20. J. Sperling, A. Perez-Leija, K. Busch, I. A. Walmsley, Quantum coherences of indistinguishable particles. *Phys. Rev. A (Coll. Park)* **96**, 032334 (2017).
21. R. Lo Franco, G. Compagno, Indistinguishability of elementary systems as a resource for quantum information processing. *Phys. Rev. Lett.* **120**, 240403 (2018).
22. A. Castellini, B. Bellomo, G. Compagno, R. Lo Franco, Activating remote entanglement in a quantum network by local counting of identical particles. *Phys. Rev. A (Coll. Park)* **99**, 062322 (2019).
23. F. Nosrati, A. Castellini, G. Compagno, R. Lo Franco, Robust entanglement preparation against noise by controlling spatial indistinguishability. *npj Quantum Inf.* **6**, 1–7 (2020).
24. F. Nosrati, A. Castellini, G. Compagno, R. Lo Franco, Dynamics of spatially indistinguishable particles and quantum entanglement protection. *Phys. Rev. A (Coll. Park)* **102**, 062429 (2020).
25. A. Perez-Leija *et al.*, Endurance of quantum coherence due to particle indistinguishability in noisy quantum networks. *npj Quantum Inf.* **4**, 1–12 (2018).
26. M. Piccolini *et al.*, Entanglement robustness via spatial deformation of identical particle wave functions. *Entropy (Basel)* **23**, 708 (2021).
27. K. Sun *et al.*, Experimental quantum entanglement and teleportation by tuning remote spatial indistinguishability of independent photons. *Opt. Lett.* **45**, 6410–6413 (2020).
28. C. Napoli *et al.*, Robustness of coherence: An operational and observable measure of quantum coherence. *Phys. Rev. Lett.* **116**, 150502 (2016).
29. M. Ringbauer *et al.*, Certification and quantification of multilevel quantum coherence. *Phys. Rev. X* **8**, 041007 (2018).
30. R. Lo Franco, G. Compagno, Quantum entanglement of identical particles by standard information-theoretic notions. *Sci. Rep.* **6**, 20603 (2016).
31. M. R. Barros *et al.*, Entangling bosons through particle indistinguishability and spatial overlap. *Opt. Express* **28**, 38083–38092 (2020).
32. S. Takeuchi, Beamlike twin-photon generation by use of type II parametric downconversion. *Opt. Lett.* **26**, 843–845 (2001).
33. T. Baumgratz, M. Cramer, M. B. Plenio, Quantifying coherence. *Phys. Rev. Lett.* **113**, 140401 (2014).
34. M. Piani *et al.*, Robustness of asymmetry and coherence of quantum states. *Phys. Rev. A (Coll. Park)* **93**, 042107 (2016).
35. I. Marvian, R. W. Spekkens, How to quantify coherence: Distinguishing speakable and unspeakable notions. *Phys. Rev. A (Coll. Park)* **94**, 052324 (2016).
36. Y.-T. Wang *et al.*, Directly measuring the degree of quantum coherence using interference fringes. *Phys. Rev. Lett.* **118**, 020403 (2017).
37. J. B. Altepeter, E. R. Jeffrey, P. G. Kwiat, Photonic state tomography. *Adv. At. Mol. Opt. Phys.* **52**, 105–159 (2005).
38. S. Gröblacher *et al.*, An experimental test of non-local realism. *Nature* **446**, 871–875 (2007).
39. J. C. Loredo *et al.*, Boson sampling with single-photon fock states from a bright solid-state source. *Phys. Rev. Lett.* **118**, 130503 (2017).
40. D. Llewellyn *et al.*, Chip-to-chip quantum teleportation and multi-photon entanglement in silicon. *Nat. Phys.* **16**, 148–153 (2020).
41. S. Wengerowsky *et al.*, Entanglement distribution over a 96-km-long submarine optical fiber. *Proc. Natl. Acad. Sci. U.S.A.* **116**, 6684–6688 (2019).
42. S. M. Barnett, S. Croke, Quantum state discrimination. *Adv. Opt. Photonics* **1**, 238–278 (2009).
43. P. J. Mosley, S. Croke, I. A. Walmsley, S. M. Barnett, Experimental realization of maximum confidence quantum state discrimination for the extraction of quantum information. *Phys. Rev. Lett.* **97**, 193601 (2006).
44. C. W. Helstrom, Quantum detection and estimation theory. *J. Stat. Phys.* **1**, 231–252 (1969).
45. A. S. Holevo, Investigations in the general theory of statistical decisions. *Proc. Steklov Inst. Math.* **124**, 1–140 (1976).
46. K. Tschernig *et al.*, Direct observation of the particle exchange phase of photons. *Nat. Photonics* **15**, 671–675 (2021).
47. R. Lo Franco, Direct measurement of fundamental statistics phase of photons. *Nat. Photonics* **15**, 638 (2021).
48. Y. Wang *et al.*, Direct measurement of particle statistical phase. arXiv [Preprint] (2022). https://arxiv.org/abs/2202.00575 (Accessed 7 February 2022).
49. L. Sansoni *et al.*, Two-particle bosonic-fermionic quantum walk via integrated photonics. *Phys. Rev. Lett.* **108**, 010502 (2012).
50. J. C. F. Matthews *et al.*, Observing fermionic statistics with photons in arbitrary processes. *Sci. Rep.* **3**, 1539 (2013).
51. F. De Nicola *et al.*, Quantum simulation of bosonic-fermionic noninteracting particles in disordered systems via a quantum walk. *Phys. Rev. A* **89**, 032322 (2014).
52. Z.-H. Liu *et al.*, Topological contextuality and anyonic statistics of photonic-encoded parafermions. *PRX Quantum* **2**, 030323 (2021).
53. S. M. Barnett, E. Riis, Experimental demonstration of polarization discrimination at the Helstrom bound. *J. Mod. Opt.* **44**, 1061–1064 (1997).
54. M. Mohseni, A. M. Steinberg, J. A. Bergou, Optical realization of optimal unambiguous discrimination for pure and mixed quantum states. *Phys. Rev. Lett.* **93**, 200403 (2004).
55. S. Sciara, R. Lo Franco, G. Compagno, Universality of Schmidt decomposition and particle identity. *Sci. Rep.* **7**, 44675 (2017).
56. P. Lodahl, A. Ludwig, R. J. Warburton, A deterministic source of single photons. *Phys. Today* **75**, 44 (2022).
57. R. Uppu, L. Midolo, X. Zhou, J. Carolan, P. Lodahl, Quantum-dot-based deterministic photon-emitter interfaces for scalable photonic quantum technology. *Nat. Nanotechnol.* **16**, 1308–1317 (2021).
58. G. Fève *et al.*, An on-demand coherent single-electron source. *Science* **316**, 1169–1172 (2007).
59. D. Press, T. D. Ladd, B. Zhang, Y. Yamamoto, Complete quantum control of a single quantum dot spin using ultrafast optical pulses. *Nature* **456**, 218–221 (2008).
60. C. Bäuerle *et al.*, Coherent control of single electrons: A review of current progress. *Rep. Prog. Phys.* **81**, 056503 (2018).
61. E. Bocquillon *et al.*, Coherence and indistinguishability of single electrons emitted by independent sources. *Science* **339**, 1054–1057 (2013).
62. M. Rashidi *et al.*, Initiating and monitoring the evolution of single electrons within atom-defined structures. *Phys. Rev. Lett.* **121**, 166801 (2018).
63. H.-L. Huang *et al.*, Emulating quantum teleportation of a Majorana zero mode qubit. *Phys. Rev. Lett.* **126**, 090502 (2021).
64. G. Compagno, A. Castellini, R. Lo Franco, Dealing with indistinguishable particles and their entanglement. *Philos. Trans. R. Soc. A Math. Phys. Eng. Sci.* **376**, 20170317 (2018).
65. A. C. Lourenço, T. Debarba, E. I. Duzzioni, Entanglement of indistinguishable particles: A comparative study. *Phys. Rev. A (Coll. Park)* **99**, 012341 (2019).
66. G. Paul, S. Das, A. Banerji, Maximum violation of monogamy of entanglement for indistinguishable particles by measures that are monogamous for distinguishable particles. *Phys. Rev. A (Coll. Park)* **104**, L010402 (2021).
67. D. Lee *et al.*, Entangling three identical particles via spatial overlap. arXiv [Preprint] (2021). https://arxiv.org/abs/2104.05937 (Accessed 18 May 2022).
68. Y. Wang *et al.*, Experimental remote entanglement distribution in a photonic quantum network through multinode indistinguishability. arXiv [Preprint] (2021). https://arxiv.org/abs/2107.03999 (Accessed 15 July 2021).